Multilayer Films Ageing Under Ultraviolet Radiations: Complementary Study by Dielectric Spectroscopy

Simon Lewandowski,[1] Virginie Rejsek-Riba,[2] Alain Bernès,[1] Sophie Perraud,[3] Colette Lacabanne[1]

[1]Physique des Polymères, Institut Carnot CIRIMAT, Université de Toulouse, 118 route de Narbonne, 31062 Toulouse Cedex 9, France
[2]ONERA, The French Aerospace Lab-DESP, F-31055 Toulouse Cedex 04, France
[3]Centre National d'Etudes Spatiales, 18 avenue Edouard Belin, 31401 Toulouse Cedex 9, France
Correspondence to: A. Bernès (E-mail: alain.bernes@univ-tlse3.fr)

ABSTRACT: The effect of ultraviolet (UV) irradiation on a multilayer film made of poly(ethylene terephthalate)/Polyamide 6/poly(ethylene terephthalate) was investigated by uniaxial tractions, UV-visible-NIR and Fourier transformed infra-red-attenuated total reflection spectroscopy, differential scanning calorimetry (DSC), and dynamic dielectric spectroscopy (DDS). The multilayer was exposed to ultraviolet radiations (filtered at 270 nm) for 7 days, in air. The complexity of the multilayer thermograms recorded by DSC and DDS has required the study of each film constituting the multilayer to assess each the contribution of each one of them. A deterioration in mechanical properties and a decrease in UV transmission for low wavelengths are observed. These evolutions seem to result to the photo-oxidation of the poly(ethylene terephthalate) film mainly localized at the exposed layer. This layer acts as a UV protection filter for the other layers. However, the DDS analyses show a plasticization effect of the primary mode in the Polyamide 6, which is evidence of photo-oxidation. © 2013 Wiley Periodicals, Inc. J. Appl. Polym. Sci. 129: 3772–3781, 2013

INTRODUCTION

Polymers films are widely used today, whether for indoor or outdoor applications, such as food containers, packing, and covering. To satisfy these large requirements, a wide range of different polymers is available to perform these films. Among them, poly(ethylene terephthalate) (PET) is one of the main polymers used as films.

Under the action of sunlight, polymer materials undergo many irreversible changes due to interactions between radiations and materials. When they have enough energy, ultraviolet (UV) radiations cause scissions of chemical bonds within polymers creating radicals: this phenomenon is called photolysis. When oxidizing agents are present in the ageing atmosphere, oxidation reactions occur after photolysis. The photo-degradation leads either a crosslinking, when we have a reaction between two radicals, or a scission, when radicals are oxidized. The main chemical changes correspond with a reduction in molecular sizes and the formation of new chemical groups within the molecules. These changes produce unwanted effects like brittleness, increase of permeability and yellowing, which are responsible for the damaging of the film integrity and the reduction in product lifetime.[1]

Numerous works published in the literature studied the chemical aspects of the polymer degradation by ultraviolet irradiation.[2–7] Photodegradation of PET and especially the resulting chemical changes were analyzed by numerous groups. Day and Wiles observed a decrease in mechanical properties at break after UV exposure. They linked these decreases to the presence of scissions in the PET chains, resulting in a decrease in number-average molecular weight.[3,4] The incidence of wavelengths was investigated. Damages are more important than the wavelengths are lower: UV < 315 nm are mainly responsible for degradations. These degradations are predominantly localized on the first micrometers of the front surface. Indeed, in the PET, it has been shown that the UV with high energy creates the scissions of chemical bonds, which are responsible of their high absorption. Therefore, this phenomenon causes a low penetration of the irradiation in film depth.[8] The presence of oxidizing agents in the atmosphere, like O_2, leads to oxidation of radicals created by scissions. This oxidation prevents the crosslinks, restricting
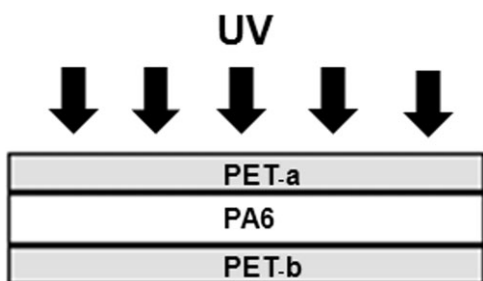
Figure 1. Multilayer film PET/PA6/PET exposed under ultraviolet radiations.

the yellowing of PET.[4] Photodegradation of the PA6 was also investigated. Indeed, two photochemistry mechanisms were observed as a function of the UV radiations wavelengths.[9,10] Through the irradiation at long wavelength (> 340 nm), a photo-initiated oxidation occurs, due to the excitation of the absorbed impurities, defects, or additives. The short wavelengths excitation produces a preponderant direct photo-scission of the NH─CO groups. Both reactions cause scissions in the PA6.

Nevertheless, only few studies showed that photodegradation produces effects on the polymer physical structure. These works revealed a change in the crystallinity and morphology. In fact, the scission of chains molecules in a semicrystalline polymer leads to their reorganization into a crystalline phase resulting in the increase of crystallinity. This phenomenon is often called chemi-crystallization which is mainly observed in polypropylene,[11,12] polyethylene,[13] and poly(ethylene terephthalate).[2] Rabello and White[12] studied the influence of photodegradation on chemi-crystallization process in polypropylene to explain the decrease in mechanical strength in the polymer film. They proposed a mechanism such as the molecule segment reorganization in the interphase region and the difference in the extent of degradation at the surface and in deeper layers. In fact, the crystallinity increasing mainly at the surface is responsible for spontaneous surface cracks causing a premature failure of polymers.

In a lot of applications, like packaging, films selected are multilayer materials. Their properties, like gas permeability or mechanical strength, are better than the monolayer film properties. Only few works were performed to study the photodegradation influence on the properties of the multilayer films.[14] This study is devoted to multilayer films constituted of a polyamide 6 film (PA6) embedded between two PET films stuck with an adhesive and labeled as PET/PA6/PET. This film was exposed to ultraviolet radiations (filtered at 270 nm) for 7 days, in a surrounding air. Our main objective is the study of UV irradiation influence on the multilayer film PET/PA/PET by uniaxial tractions, UV-visible (UV-Vis), and Fourier transformed infra-red-attenuated total reflection (ATR) spectroscopy. Moreover, the originality of this work is to study also the molecular mobility evolution by dynamic dielectric spectroscopy (DDS).

EXPERIMENTAL

Materials
Multilayer films used in this study were manufactured with a Polyamide 6 (thickness of 20 μm) bonded between two PET

films (thickness of 15 μm each one) with poly(urethane) adhesive. The multilayer film had a total thickness of 53 μm.

The Polyamide 6 (PA6) used was a biaxially oriented film produced by double bubble extrusion technology. The PET was a biaxially oriented film produced in a two-step-stretching process: the first, in the travel direction, and the second, in the transverse direction. The poly(urethane) adhesive was a bi-component thermosetting system which offer good low-temperature adhesion coupled with good flexibility and toughness. The side of the film directly exposed to the ultraviolet radiations is name PET-a, as shown in Figure 1.

Ultraviolet Irradiation
UV irradiation was achieved by a short arc Xenon lamp with filter. This system (lamp + filter) produces ultraviolet light from 270 to 400 nm. The irradiance spectrum of this light source is reported in Figure 2. Films were placed in a hermetic chamber. The ageing cycle was performed at a temperature of 23°C in a surrounding air at 1 atm during 7 days.

Mechanical Properties Measurements
The mechanical properties measurements were tested in a Instron 5569 machine operating with a 1 kN lead cell and a crosshead speed of 100 mm min^{-1} at room temperature. The sizes of the test specimen were 20 mm wide and 200 mm long with a 100 mm clamp separation. Tensile measurements were performed in traverse direction. The values of tensile strength, maximum elongation, and Young's modulus reported in this study correspond to averages calculated with the results obtained for a number at least of five samples.

UV-Vis-NIR Spectroscopy
UV-Vis-NIR spectra were recorded with a Perkin Elmer Lambda 900 UV-Vis spectrometer associated with a 150 mm diameter integrating sphere, recovered by Spectralon, in air. The transmission measurements were performed for each sample. The calibration curve was done with a diffuser Spectralon standard.

FTIR-ATR
Films were analyzed by FTIR spectroscopy using a Nicolet 800 spectrometer in the range of 400–4000 cm^{-1}, with a resolution
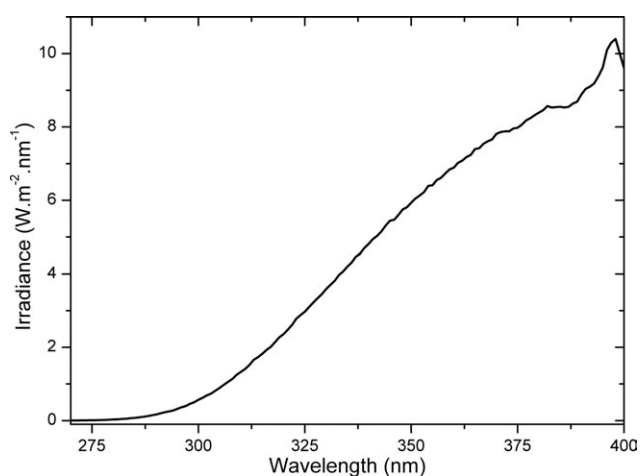

Figure 2. Irradiance curve for the light source.

of 4 cm^{-1}. An attenuated total reflection (ATR) accessory was used to quantify the degradation at the surface layers. The FTIR-ATR technique allowed to investigate the first micrometer of the multilayer surfaces.

Differential Scanning Calorimetry

Differential scanning calorimetry (DSC) measurements were performed with a TA instrument (2920 CE). Films were analyzed in nonhermetically sealed aluminum pans. The sample weight was ranging from 5 to 10 mg. Thermograms were recorded at a heating rate of 10°C min^{-1} in temperature range from −50 to +300°C, under a dry helium gas purge at a flow rate of 110 mL min^{-1}. High purity indium and mercury were used for temperature and enthalpy calibration.

The melting temperature (T_m) was taken at the maximum of the endothermic peak and the enthalpy variation calculated from the peak area. We evaluated the degree of crystallinity of PET and PA6 films, using eq. (1):

$$\chi_c^{PET} = \Delta H_{f,net}/\Delta H_o \quad (1)$$

where ΔH_0 is the heat of fusion of an ideal 100% crystalline, and $\Delta H_{f,net} = \Delta H_f - \Delta H_c$ is the net heat of fusion with ΔH_f being the heat of fusion, and ΔH_c being the heat of crystallization. A value of $\Delta H_0 = 140$ J g^{-1} was used for PET and a value of $\Delta H_0 = 257$ J g^{-1} was used for PA6.[15]

DDS

To determine the molecular mobility, the measurements of the complex dielectric permittivity $\varepsilon^\star$ were performed with a Novocontrol Broadband Dielectric Spectrometer (BDS4000), in the frequency range of 10^{-2} to 10^6 Hz.

$$\varepsilon^*(F) = \varepsilon'(F) - i\varepsilon''(F) \quad (2)$$

Experiments were performed isothermally from −150 to +150°C by steps of 5°C. The temperature in the cryostat was controlled with a stability of ±0.5°C by a cold nitrogen gas stream, heated by a Quatro temperature controller. Samples were placed between gold-plated stainless steel electrodes (Ø = 20 mm).

The experimental limit for the loss factor ε" was about 10^{-4}.

The real ε' and imaginary ε'' parts of the relative complex permittivity $\varepsilon^\star$ were measured as a function of frequency F at a given temperature T. From each isothermal plot, the relaxation modes were described by the double-stretched Havriliak–Negami function.

$$\varepsilon^*(\omega) = \varepsilon_\infty + \frac{\varepsilon_S - \varepsilon_\infty}{[1 + (i\omega\tau_{HN})^{\alpha_{HN}}]^{\beta_{HN}}} \quad (3)$$

where ω is the angular frequency ($\omega = 2\pi F$), ε_s and ε_8 are the relaxed ($\omega = 0$) and unrelaxed ($\omega = 8$) dielectric constants, t_{HN} is the relaxation time of Havriliak–Negami (HN) model. The exponents α_{HN} and β_{HN} characterize the width and the asymmetry of the relaxation time distribution respectively. At each temperature, a value of t_{HN} was found for the modes present in the frequency window used here. The relaxation diagrams were

plotted representing the variations of log$\tau_{HN}(1/T)$ which are expected to be linear in the case of Arrhenius dependences for the relaxation time [eq. (4)] and curved for Vogel–Tammann–Fulcher (VTF) ones [eq. (5)], according to the following expressions:

$$\tau_{HN}(T) = \tau_0 \exp\left(\frac{E_a}{RT}\right) \quad (4)$$

$$\tau_{HN}(T) = \tau_{0v} \exp\left(\frac{1}{\alpha_f(T - T_\infty)}\right) \quad (5)$$

where t_0 and t_{0v} are the pre-exponential factors, E_a the activation energy and R the ideal gas constant, α_f the thermal expansion coefficient of the free volume, and T_∞ is the critical temperature at which any mobility is frozen. We must take the fitting procedure into account because very often incomplete peaks appear despite the extension of frequency window in eight decades range. As the temperature increases, the relaxation peaks shift to higher frequencies and sweep the frequency window with different speeds characteristic of the relaxation energy of each mode.

The fittings were performed with the nonlinear last-squares standard procedure Winfit from Novocontrol, starting from different initial parameters.

RESULTS AND DISCUSSION

We studied the degradation induced by UV exposition through several methods. The complexity of the thermal and dielectric properties of the multilayer film requires the study of each film constituting the multilayer to assess each one of their contribution.

Mechanical Properties

Young's modulus, stress, and strain at break were especially investigated. The typical stress–strain curves of the multilayer film before and after UV exposition are represented Figure 3. The data obtained for the multilayer before and after UV exposition are reported in Table I. Stress and strain at break present
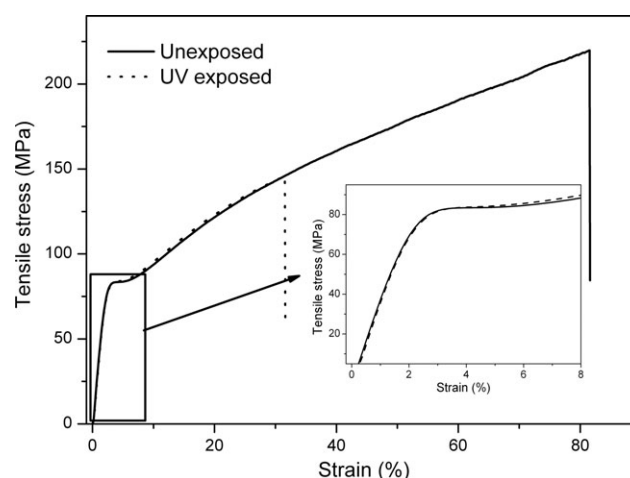

Figure 3. Tensile stress–strain curves of unexposed and UV exposed multilayer films.

Table I. Failure Mechanical Properties Performed in Unexposed and UV Exposed Multilayer Films

Multilayer films	Stress at break (MPa)	Strain at break (%)	Young's modulus (MPa)
Unexposed	222 ± 20	85 ± 10	3970 ± 31
UV exposed (UV, +23°C, atm, 7 days)	145 ± 6	32 ± 3	4021 ± 46

a significant decrease after UV irradiation. Young's modulus is almost unaffected. Several studies showed a large deterioration in mechanical properties of PET film or multilayers film based on PET.[4,5,14]

Thermo-Optical Properties

The UV-Vis spectra of unexposed and UV exposed multilayer films reported in Figure 4 show a decrease in transmission after irradiation and a shift of the UV cut off toward the high wavelengths.

A slight yellowing of the film is observed for the multilayer exposed under the UV. Using UV-Vis spectroscopy allows estimating this yellowing by the increase in the absorption at 400 nm.[2] In our multilayer, this phenomenon is observed on Figure 4, where the UV-Vis transmission decreases after irradiation. In the literature, this evolution has been ascribed to quinone and diquinone formed during the photodegradation of PET.[1,5]

Chemical Modifications

The layer PET-b studied after the irradiation is not altered. Nevertheless, changes in the PET-a spectra are observed in Figure 5 around 2500–3750 cm^{-1}, region assigned to —OH stretching vibrations absorption bands. Day and Wiles have identified the origin of the different absorption bands attributed to O-H stretching vibration of the aqueous, alcoholic, and carboxylic acid functional groups. From their work, the absorption bands at 3620 cm^{-1} and 3550 cm^{-1} can be assigned to the stretching vibration of absorbed H_2O molecules in PET films and the alcoholic O—H stretching respectively, and the absorption band at
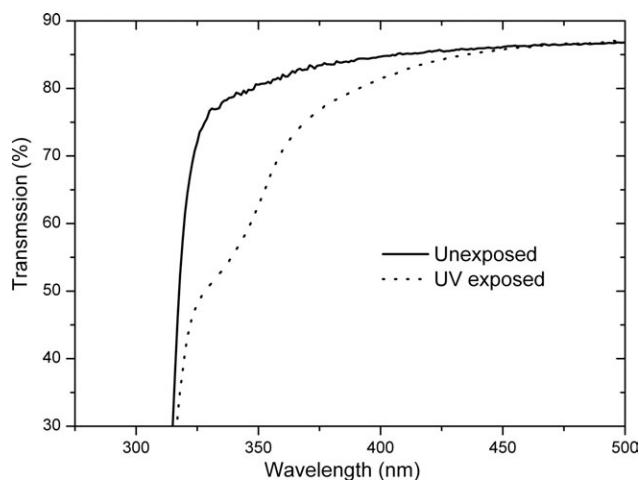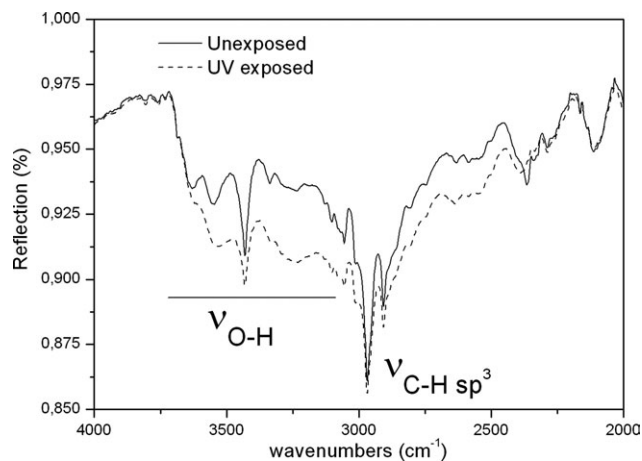
Figure 5. FTIR-ATR spectra of unexposed and UV exposed multilayer films.

3290 cm^{-1} can be attributed to the carboxylic O—H stretching vibration.[3–5] The absorption band centered at 3290 cm^{-1} was found to be favorably situated to provide a quantitative estimate of the —COOH end-groups. The peak centered at 2970 cm^{-1} corresponding to C—H absorption, is usually considered as a reference. We note after irradiation that the normalized ratio of the —OH absorption to the C—H absorption is increasing, which can be attributed to the increase in the concentration of the carboxyl end-groups.

This study by FTIR-ATR spectroscopy allows to show that only the PET-a of the multilayer, directly exposed to UV irradiation, is affected by the degradation of its chemical structure. Indeed, the surface spectra of the PET-a layer measured by means of FTIR-ATR show on Figure 5 an increase in the intensity of the —OH stretching vibrations of the carboxylic acid end-groups. According to the literature, under surrounding air conditions, the photochemical reactions give rise to chain scissions and formation of carboxyl end-groups.[3,16,17] It is also well known that the carboxyl end-groups act as catalyst to promote further degradation.[1] These phenomena observed are in agreement with the mechanical results. Indeed, the extensive chemical degradation, resulting in chain scission reactions and the formation of carboxyl end-group, is responsible for the decrease in mechanical properties at break while the Young's modulus is not affected (Table I).

Thermal Transitions

To identify each event observed in these complex thermograms (Figure 6, unexposed multilayers) and assign them to the different layers of the multilayer, separated elements have been investigated.

The DSC thermograms shown in Figure 6 were recorded on unexposed multilayer, PA6, PET, and adhesive. The first heating run (curve a) performed on initial sample of multilayer film reveals a broad endothermic peak centered at 80°C, followed by two endothermic peaks at 220°C and 255°C. In the second heating run (curve b) performed immediately after cooling from 280°C, the broad peak at 80°C disappears, whereas the two higher peaks are always observed.
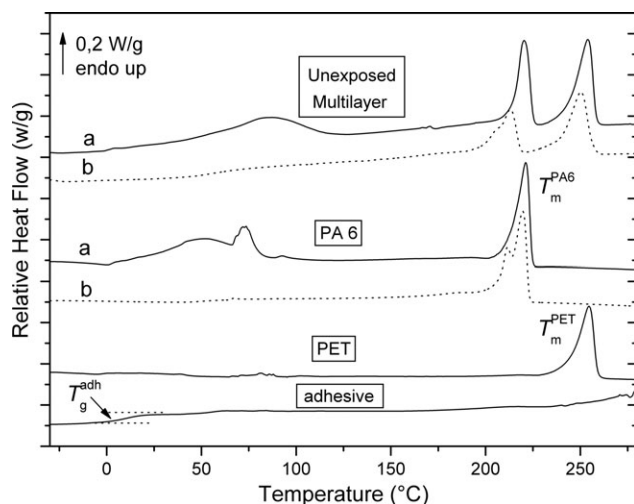
Figure 4. UV-Vis spectra of unexposed and UV exposed multilayer films.

Figure 6. DSC thermograms of unexposed multilayer film and its constitutive layers: PA6, PET, and adhesive (curve a: first run, curve b: second run).

The first heating run performed on initial sample of PA6 (curve a) reveals a broad endothermic peak around 60°C and an endothermic peak at $T_m^{PA6} = 220$°C. The peak T_m^{PA6} situated at the highest temperature correspond to the melting of the crystalline phase in PA6.[18] In the second heating run (curve b), the broad peak at 60°C disappears. The PA6 film is well known as a hygroscopic polymer. This broad peak observed above the room temperature reveals desorption of water in the film during the heating run.

The thermogram of PET shows clearly an endothermic peak at $T_m^{PET} = 255$°C corresponding to its melting point.[19] The glass transition region is unapparent, due to the semicrystalline morphology of the film. Between 30 and 120°C, slight endothermic events are observed, characteristic of water evaporation.

The thermogram of adhesive highlights a step of heat flow around the room temperature, which is characteristic of the adhesive glass transition T_g^{Adh}, defined as the midpoint of the step of heat capacity, at 5°C.

The broad endothermic peak presents in the multilayer film thermogram has intensity and a behavior similar to the peak observed in PA6 thermogram. This indicates that this peak observed in the multilayer is mainly due to the evaporation of water present in the PA6 layer. We note the shift of this peak toward higher temperature in the multilayer. This phenomenon can be attributed to the confined situation of the PA6 film between the two PET films, where the water is hampered to diffuse. The two peaks observed at 220 and 255°C on the DSC thermogram of the multilayer film are attributed to PA6 and PET melting peaks, respectively. The thermogram of the unexposed multilayer (Figure 6; curve a) allows to calculate the crystallinity rate of the PET layers and the PA 6 layer, using eq. (1). The values obtained are $\chi_c^{PET} = 31\%$ and $\chi_c^{PA6} = 23\%$.

The crystalline phases of PET and PA6 seem to be not affected by the UV irradiations ($\chi_c^{PET} = 32\%$, $T_m^{PET} = 255$°C; $\chi_c^{PA6} = 21\%$, $T_m^{PA6} = 220$°C). Fechine et al.[2] studied the structural

Table II. Dielectric Relaxation Modes Designation

	Secondary relaxation modes		Primary relaxation modes (u = upper, L = lower)	
Unexposed multilayer	γ^{UnM}	β^{UnM}	α_L^{UnM}	α_u^{UnM}
UV exposed multilayer	γ^{EM}	β^{EM}	α_L^{EM}	α_u^{EM}
PET	–	β^{PET}	α_L^{PET}	–
PA6	γ^{PA6}	β^{PA6}	α_L^{PA6}	α_u^{PA6}
adhesive	γ^{Adh}	β^{Adh}	α_L^{Adh}	α_u^{Adh}

changes during photodegradation of PET and observed a 2.5°C decreasing of the melting peak of PET after 25 days of exposure. The exposure time selected for this study is too weak to observe a significant shift of melting peak and an evolution of crystallinity rate. Indeed, this is for a longer ageing time performed with similar conditions that allowed to observe a temperature decreasing of the PET melting peak.[2]

Dielectric Relaxations

The dielectric loss ε'' was recorded by using DDS on unexposed and UV exposed multilayer films for temperature range −150 to 150°C and frequency range 10^{-2} and 10^6 Hz. All the dielectric relaxation modes studied in this dielectric section are resumed in the Table II. The dielectric loss surface of unexposed multilayer film is shown in Figure 7. This 3D representation reveals at low temperature two secondary relaxation modes γ^{UnM} and β^{UnM}, then at higher temperature two primary relaxation modes α_L^{UnM} and α_u^{UnM}. The spectrum obtained reveals the existence of
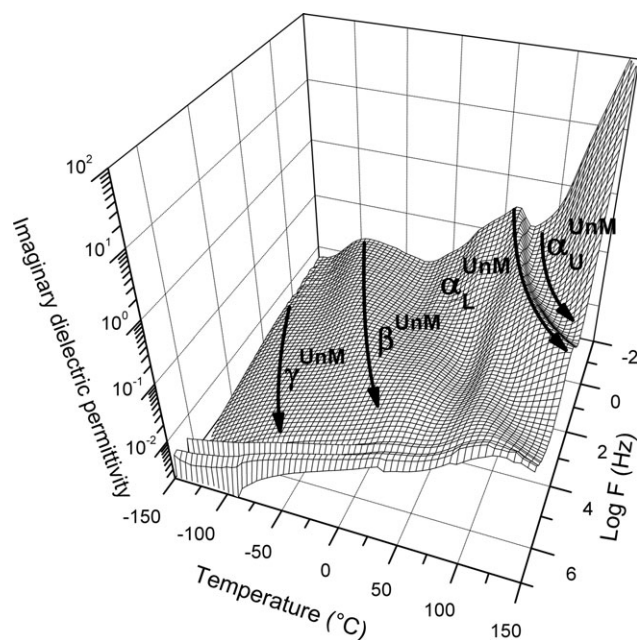

Figure 7. Dielectric loss surface of unexposed multilayer film obtained by DDS.
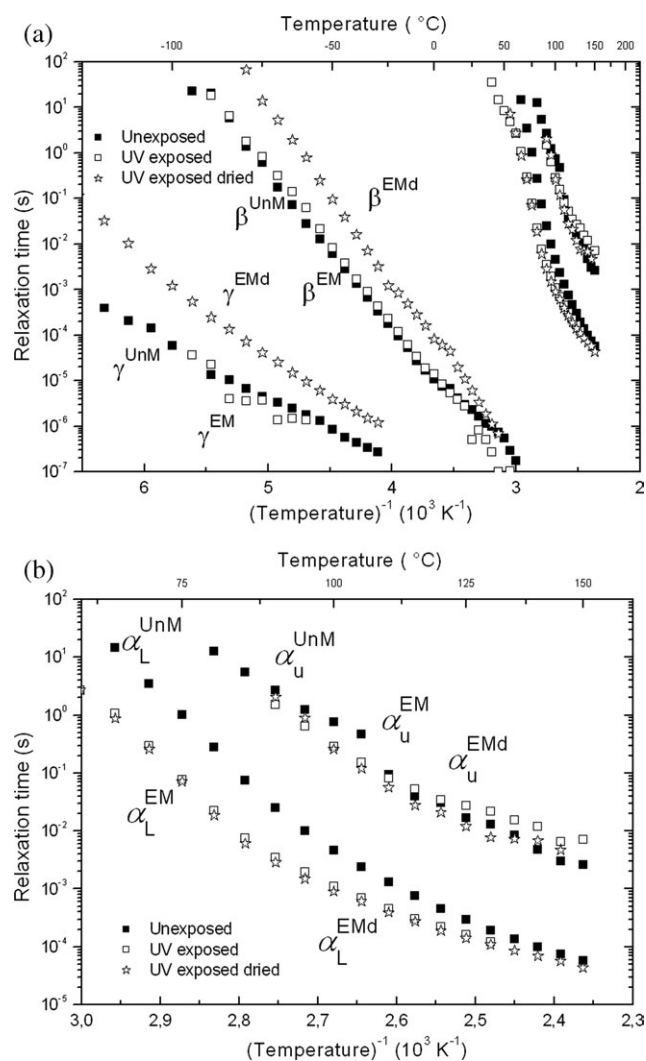
Figure 8. (a) Arrhenius diagram of relaxation times of multilayer before and after UV exposure. (b) Arrhenius diagram of relaxation times at high temperature of multilayer before and after UV exposure.

discrete dipolar relaxation modes, and the dielectric relation times t_{HN} extracted from each complex relaxation modes have been reported in the Arrhenius diagrams [filled squares in Figure 8(a)]. For comparison, the t_{HN} values of the exposed multilayer have been also shown in Figure 8(a), where the primary and secondary relaxation modes are labeled as EM. The temperature dependences of the dielectric relaxation situated at the lowest temperatures of the Arrhenius diagram reveal that the γ^{UnM} and β^{UnM} modes are not affected by the UV irradiation during 7 days. The primary relaxation modes obtained at the highest temperature was reported in the large-scale Figure 8(b). This Arrhenius diagram highlights the relaxation mode α_L^{UnM} is significantly shifted toward the lower temperatures after the UV irradiation, whereas the α_u^{UnM} mode is not affected.

In polymers as the PA6, the intra- and interchain hydrogen bonds play an important role in the dielectric relaxation occurring when water molecules enter the material.[20] To verify that the dielectric relaxation time variations observed after UV irradiation [Figure 8(a,b)] is not due to the water, a dried

irradiated multilayer has been studied by DDS. Irradiated multilayer was dried at room temperature by a powerful desiccant, the phosphorus pentoxide (P_2O_5) salt. The Havriliak–Negami relaxation times extracted, for each relaxation mode, are reported for the dried irradiated multilayer in the Arrhenius diagrams of Figure 8(a,b) (represented by open star). We observe, for the drying exposed sample, a shift of the two secondary relaxation modes, γ^{EMd} and β^{EMd}, relaxation times toward higher temperatures [Figure 8(a)]. In opposite, the relaxation times of the two primary modes, α_L^{EMd} and α_u^{EMd}, are not modified [Figure 8(b)]. During the record of the primary relaxation modes, the DDS experimental conditions impose several isothermal programs above the room temperature. At this stage, water molecules are susceptible to leave the sample. Therefore, the similar behavior of the primary relaxation modes observed for the undried and dried irradiated multilayers, in Figure 8(b), can be explain by these experimental conditions. At temperatures higher than 55°C, both samples have a similar state of drying. These results confirm that the evolution of the dielectric relaxations observed after irradiation in Arrhenius diagram, Figure 8(a,b), is characteristic of the UV radiations incidence on molecular mobility.

The evolution observed on the α_L^{UnM} indicates that modifications occur during the UV exposition. To identify the element of the multilayer which is involved, a study of each film constituting the multilayer has been performed. The variation of the dielectric loss ε'' was recorded between 10^{-2} and 10^6 Hz, and -150 and $150°C$. The t_{HN} values extracted from each complex relaxation modes are shown in the Arrhenius diagrams [filled squares for unexposed multilayer in Figure 9(a)]. For comparison, variation of relaxation time obtained on the films constituting the multilayer, PA6, PET, and adhesive, indicated by open squares, open triangles, and open circles, respectively [Figure 9(a,b)] are also reported in these Arrhenius diagrams.

This diagram reveals below the room temperature several secondary dielectric relaxation modes of which some were already observed: two secondary relaxations γ^{PA6} and β^{PA6} obtained in the PA6 film,[20] a wide secondary relaxation β^{PET} for the PET film[19] and for the adhesive the two relaxation modes γ^{Adh} and β^{Adh}. These modes are well fitted by an Arrhenius law, whose corresponding parameters are reported in Table III. We note that the secondary relaxation modes are associated to the low values of the activation enthalpy which are characteristic of localized motions. In the PA6, the β^{PA6} relaxation process is commonly related to labile amide group motions.[21,22] The γ^{PA6} relaxation involves local movements of sequences of four or six methylene units.[21] Because the γ^{PA6} relaxation is dielectrically active, the motions must also involve some amide groups. A previous dielectric study shows in the PET, the broad secondary mode, β^{PET}, is constituted of two components[23]: the low temperature component involves noncooperative mobility of the carbonyl groups motions, whereas the relaxation process ascribed to the high temperature component corresponds to the local motions of the phenyl rings proceeded in a cooperative way.

We note also the primary dielectric mode α_L^{Adh} of the adhesive. Indeed, the variation of relaxation time of the α_L^{Adh} is well
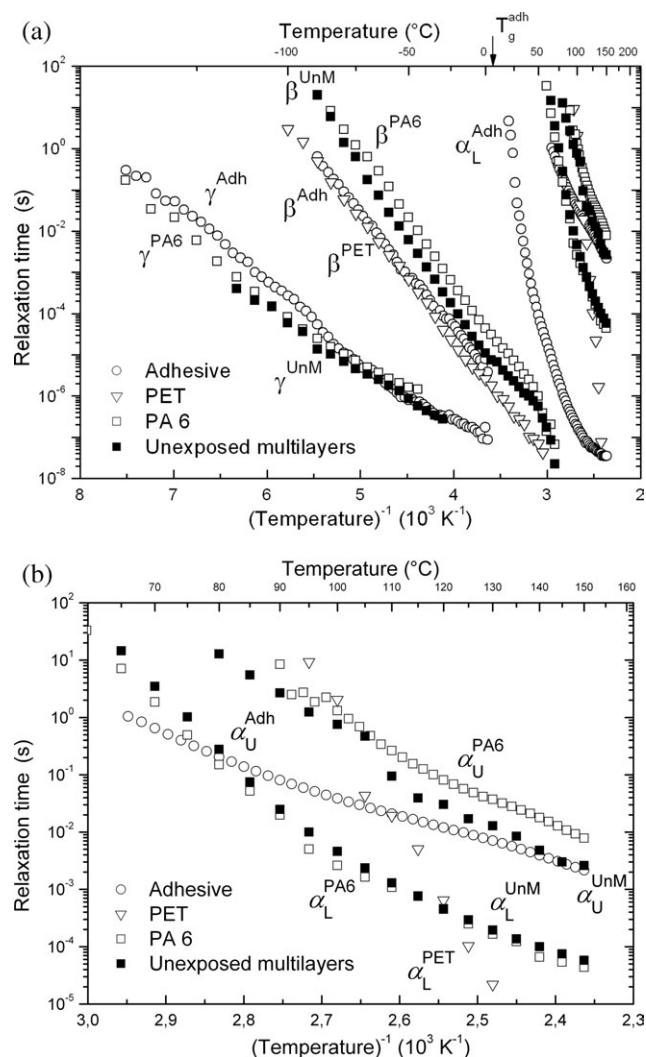
Figure 9. (a) Arrhenius diagram of relaxation times for unexposed multilayer film and its constitutive layers: PA6, PET, and adhesive. (b) Arrhenius diagram of relaxation times situated at high temperature for unexposed multilayer film and its constitutive layers: PA6, PET, and adhesive.

described by a VTF law [eq. (5)] with parameters values $\tau_{0v} = (8 \pm 1.5) \times 10^{-11}$ s, $\alpha_f = (1 \pm 0.05) \times 10^{-3}$ K^{-1}, and $T_8 = 255 \pm 1$ K, usually observed in the glass transition region. Its extrapolation at 10^2 s, a characteristic time of the glass transition, agrees with the glass transition temperature of the adhesive, T_g^{Adh}, obtained by DSC (Figure 5).

The primary relaxation modes obtained at higher temperature above the α_L^{Adh}, were reported in the large-scale Figure 9(b). We note the variations of relaxation times α_L^{UnM} is well described by a VTF law with parameters values $\tau_{0v} = (1 \pm 0.7) \times 10^{-8}$ s, $\alpha_f = (8 \pm 0.6) \times 10^{-4}$ K^{-1}, and $T_8 = 282 \pm 3$ K, whereas the α_u^{UnM} mode shows an Arrhenius dependence with the activation energy and the pre-exponential factor values reported in Table III. This diagram shows that the variation of relaxation time obtained on unexposed multilayer, α_L^{UnM}, coincide with the variation of the PA6, α_L^{PA6}, but it is different from the temperature

dependences of PET, α_L^{PET}. The primary mode α_L^{PA6} and α_L^{PET} has been ascribed to the dielectric manifestation of the glass transition in PA6[20] and PET,[19] respectively.

Above these primary modes, the upper modes, α_u^{PA6} and α_u^{PET}, are fitted by an Arrhenius law which have been already observed.[19,20] The upper mode was also studied in the PET by mechanical means[24] and dielectric techniques,[25] where its real nature is often discussed. Up to now, we still do not know the origin of this mode, but its dielectric manifestation can be related directly (dipolar) or indirectly (ionic) to a motion of macromolecular chains.[25] These bimodal relaxations α_L^{PA6} and α_u^{PA6} for the PA6, then α_L^{PET} and α_u^{PET} for PET, are situated around and above the glass transition, respectively, are significant amorphous phase heterogeneity in semicrystalline polymers. Several authors have shown the properties of semicrystalline polymers can be explained by a three-phase model: besides crystalline and mobile amorphous phase (MAP), there is a third phase called rigid amorphous phase (RAP).[26–28] According to this assumption, the α_L^{PA6} and α_L^{PET} modes are attributed to the MAP responsible for the glass transition observed by DSC measurements, whereas the α_u^{PA6} and α_u^{PET} modes are ascribed to the RAP where the amorphous phase is constrained by crystalline lamellae. The urethane adhesive reveals also an upper component α_u^{Adh} in Figure 9(b), which could be attributed to microstructural entities corresponding to a local order of the amorphous phase. Schmieder and Wolf[29] were the first authors to propose the assumption where such entities would be responsible for mechanical bimodal relaxations associated with a double glass transition in the polyvinyl chloride. On a molecular scale, these authors attributed these entities to syndiotactic sequences, segregated into domain of upper glass transition due to high level of local order. In the polycarbonate an upper-temperature component was also observed upon annealing above the glass transition.[30] This component has been assigned to a constrained amorphous phase where local order of some

Table III. Arrhenius Parameters for the Unexposed and UV Exposed Multilayer Films, PA6, PET, and Adhesive

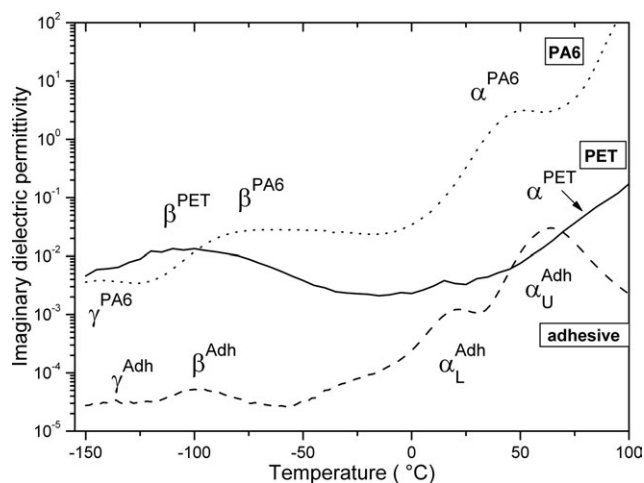|	τ_O (s)	E_a (kJ mol^{-1})
Unexposed multilayer		
γ^{UnM} mode	$(3 \pm 1)\,10^{-13}$	27 ± 0.5
β^{UnM} mode	$(5 \pm 3)\,10^{-18}$	64 ± 0.7
α_u^{UnM} mode	$(5 \pm 3)\,10^{-23}$	157 ± 6
PA6		
γ^{PA6} mode	$(5 \pm 3.7)\,10^{-14}$	31 ± 0.8
β^{PA6} mode	$(2 \pm 0.4)\,10^{-16}$	60 ± 0.4
α_u^{PA6} mode	$(7 \pm 0.8)\,10^{-20}$	137 ± 3.7
PET		
β^{PET} mode	$(5 \pm 1)\,10^{-17}$	56 ± 0.4
Adhesive		
γ^{Adh} mode	$(1 \pm 0.4)\,10^{-14}$	34 ± 0.4
β^{Adh} mode	$(3 \pm 0.6)\,10^{-16}$	53 ± 0.3
α_u^{Adh} mode	$(1 \pm 0.5)\,10^{-13}$	83 ± 1.2

Figure 10. Superposition of the imaginary dielectric permittivity upon temperature obtained at the frequency $F = 10^{-1}$ Hz for each polymer PA6, PET, and adhesive.

4 nm is induced by the stiffness of the bisphenol A sequence. In the urethane adhesive, a significant heterogeneity of the amorphous phase could be produce during the crosslink process. Nevertheless, it is not possible to specify the characteristics of the local order.

The Arrhenius diagrams, Figure 9(a,b), show a similar behavior of the dielectric relaxation modes between γ^{UnM} and γ^{PA6}, and then between α_L^{UnM} and α_L^{PA6}. Although the modes β^{UnM} and α_u^{UnM} are close to the β^{PA6} and α_u^{PA6}, respectively, we can deduce that the characteristic of the dielectric relaxation spectrum of the multilayer (Figure 7) correspond mainly to the ones of the PA6. To verify this assumption, we have superimposed in Figure 10 the variation of the imaginary dielectric permittivity upon temperature obtained at the frequency $F = 10^{-1}$ Hz for each polymer PA6, PET, and adhesive constituting the multilayer. This diagram allows us to show that the PA6 spectrum seems to have an intensity dominating in comparison with each spectrum of the PET and adhesive. We can conclude that the multilayer dielectric spectra are characteristic of PA6 one. Therefore, in the following, we assume the behavior of the dielectric mode α_L^{UnM} can be considered as representative of the α_L^{PA6}. The α_u^{UnM} mode of the multilayer situated in the temperature region of the PA6 mode α_u^{PA6}, is characteristic of the RAP constrained by crystalline lamellae. The assignment of the γ^{UnM} and β^{UnM} multilayer modes to the ones of PA6, γ^{PA6}, and β^{PA6} modes, respectively, allows to explain the unplasticization effect observed on the secondary dielectric relaxation processes after the drying in Arrhenius diagram of the Figure 8(a). Indeed, plasticization of polyamide was interpreted[31] as the result of two effects: (i) the reduction of interchain bonding (decrease in interchain forces) by replacement of amide–amide hydrogen bonds by hydrogen bonded water molecules, and (ii) the increase of the segmental mobility by dilution. Therefore, the temperature increasing of the γ^{UnM} and β^{UnM} modes after drying [Figure 8(a)] reveals the role of the water molecules to facilitate the local molecular mobility in the PA6 constituting the initial multilayer film.

Influence of Photodegradation on Molecular Mobility in the PA6 Layer

The study by DDS indicates that the DDS spectra of the multilayer allow to investigate the PA6 film. These dielectric relaxations reveal that the UV irradiations are responsible for the decrease in the primary relaxation mode temperature α_L^{UnM} [Figure 8(b)], therefore of this one of α_L^{PA6}. Several studies[32] have shown that the main-chain motions responsible for the primary mode in the polyamides must involve the rupture of hydrogen bonds (amide–amide hydrogen bonds or hydrogen bonded water molecules) in the amorphous phase. UV irradiation causes scissions of the main-chains in the PA6 which provoke the formation of new radicals. These processes lead to two possible mechanisms. The first assumption is that water molecules could be attached themselves to these radicals with a weak bound. The bonded water molecules have consequences for create spacing out interchain. The decrease in the interchain cohesive forces resulting from a lower density of chains could be responsible for the shift of the primary mode to lower temperature. The second assumption is that the radicals are oxidized by the oxygen present in the atmosphere, which causes scissions due to —OH ending. The scissions of the main-chains cause also a greater mobility of the macromolecules.

Crosslinking of such radicals seems to be insignificant, as it would cause a shift of the primary mode toward higher temperatures due to the creation of new bonds. We note, this phenomenon is not observed in the Figure 8(b). Then, we think the crosslinking is not effective, probably due to the low density of the radicals created, diminishing in this way the possibility of the two radicals proximity.

It must be recalled that plasticization effects induced by water molecules is stronger in polyamides with short polymethylene sequences (polyamide 5, 6, 6-6, 7…) due to their higher hydrophilic character.[33] There are numerous possible ways in which a water molecule may be bonded to or between carbonyl and amide groups. It is interesting to note that several authors have shown that the clustering of water molecules occurs at a water concentration near one molecule per two amide groups in the amorphous regions.[21] Therefore, we propose that the drying performed, on one hand, by the desiccant, P_2O_5 salt at room temperature, and, on the other hand, by the thermal program during the recording of DSC thermograms and DDS spectra, allow to remove alone water molecules present in the cluster. On the contrary, the bounded water molecules should not be affected by this drying. Indeed, McCrum et al.[32] have shown that a drying prolonged time during several days at higher temperature (150°C) in vacuum over calcium chloride is required to remove them.

It is interesting to note in the exposed multilayer, the UV radiations modify the cooperative molecular mobility around the glass transition in the PA6, whereas the localized entities mobility in the PA6 are not affected as the γ^{EM} and β^{EM} modes show it [Figure 8(a)]. In a previous work, we have studied by dielectric relaxation the incidence of the complex chain architectures on the molecular mobility.[34] Hence, at low temperatures, the localized molecular mobility observed, through the secondary

relaxation modes, involves mainly the movements of the side groups characterized by an activation entropy close to zero. When the temperature increases, the primary mode involves the main-chain and, more precisely, longer and longer sequences of this chain. By using the concept of domains, we have shown that the dielectric relaxation studied, probe larger and larger domains, as the temperature is increasing, but inside these domains, sequences move cooperatively with an activation enthalpy and entropy that increase with regard to the size of the domains. In agreement with the previous assumption where the low density of the radicals created is established, the average distance between the radicals is the same size of the one of the cooperative domains associated with the primary mode of the PA6. Therefore, this average distance between the radicals is sufficiently large to influence the delocalized molecular mobility around the glass transition, but this phenomenon does not affect the low size relaxing units constituting the secondary mode.

At higher temperatures, the RAP is not affected by UV radiations as it is the case for the crystalline phase which has not evolved after the analysis by DSC. This result seems to be in agreement with the proposition where UV radiations can have difficulties to affect the rigid chains segment, due also to the high level of the amorphous phase density in the RAP.

CONCLUSION

The analytical study of a new multilayer film PET/PA6/PET after UV exposition has been realized. The macroscopic properties are affected, with a decrease of mechanical properties at break and a decrease in UV transmission for low wavelengths. These modifications are similar to these observed on single PET film or other PET based multilayer films. These observations were confirmed by ATR-FTIR spectroscopy of the PET situated in front of the UV radiations, which shows a decrease in reflexion of the band at 3290 cm^{-1}, traducing scissions in PET. Due to the low penetration of destructive UV inside the PET, the front layer should act as protective filter for the multilayer.

The DDS allowed to study the PA6 layer, situated between two PET films. This experimental protocol allows to detect the presence of a plasticizing effect of the PA6 primary mode. Despite the protection of PET layers, a photo-oxidation seems to occur in the PA6 layer. On the contrary, the localized molecular mobility, characteristic of the secondary relaxation modes, is not affected by UV irradiation. In that case, the study by dielectric spectroscopy reveals that the UV radiations cause the evolution of the nanometric domains structure, characteristic of the sequences moving cooperatively around the glass transition. Nevertheless a complementary study would be necessary to identify the exact process responsible for this plasticizing effect.

ACKNOWLEDGMENTS

REFERENCES

1. Rabek, J. F. Polymer Photodegradation: Mechanisms and Experimental Methods; Chapman and Hall: London, **1995.**

2. Fechine, G. J. M.; Souto-Maior, R. M.; Rabello, M. S. *J. Mater. Sci.* **2002,** *37*, 4979.

3. Day, M.; Wiles, D. M. *J. Appl. Polym. Sci.* **1972,** *16*, 175.

4. Day, M.; Wiles, D. M. *J. Appl. Polym. Sci.* **1972,** *16*, 191.

5. Fechine, G. J. M.; Rabello, M. S.; Souto-Maior, R. M. *Polym. Degrad. Stab.* **2002,** *75*, 153.

6. Wang, W.; Taniguchi, A.; Fukuhara, M.; Okada, T. *J. Appl. Polym. Sci.* **1998,** *67*, 705.

7. Wang, W.; Taniguchi, A.; Fukuhara, M.; Okada, T. *J. Appl. Polym. Sci.* **1999,** *74*, 306.

8. Eickmeier, A.; Bahners, T.; Schollmeyer, E. *J. Appl. Phys.* **1991,** *70*, 5221.

9. Lemaire, J.; Gardette, J. L.; Rivaton, A.; Roger, A. *Polym. Degrad. Stab.* **1986,** *15*, 1.

10. Roger, A.; Sallet, D.; Lemaire, J. *Macromolecules* **1986,** *19*, 579.

11. Mani, R.; Singh, R. P.; Sivaram, S.; Lacoste, J. *Polym. J.* **1994,** *26*, 1132.

12. Rabello, M. S.; White, J. R. *Polymer* **1997,** *38*, 6379.

13. Albertsson, A. C.; Barenstedt, C.; Karlsson, S. *Polym. Degrad. Stab.* **1992,** *37*, 163.

14. Fechine, G. J. M.; Souto-Maior, R. M.; Rabello, M. S. *J. Appl. Polym. Sci.* **2007,** *104*, 51.

15. Wunderlich, B., Eds. Thermal Analysis, Academic Press: San Diego, **1990;** pp 424.

16. Day, M.; Wiles, D. M. *J. Appl. Polym. Sci.* **1972,** *16*, 203.

17. Allen, N. S.; Edge, M.; Mohammadian, M. *Polym. Degrad. Stab.* **1994,** *43*, 229.

18. Xenopoulos, A.; Wunderlich, B. *J. Polym. Sci. Part B: Polym. Phys.* **1990,** *28*, 2271.

19. Carsalade, E.; Bernes, A.; Lacabanne, C.; Perraud, S.; Lafourcade, M.; Savignac, M. *J. Therm. Anal. Calorim.* **2010,** *101*, 849.

20. Laredo, E.; Grimau, M.; Sanchez, F.; Bello, A. *Macromolecules* **2003,** *36*, 9840.

21. Starkweather, H. W. In Water in Polymers; Rowland, S. P., Eds.; American Chemical Society: Washington, D.C., **1979;** Chapter 25, pp 433.

22. Demont, P.; Diffalah, M.; Martinezvega, J. J.; Lacabanne, C. *J. Non-Cryst. Solids* **1994,** *172*, 978.

23. Menegotto, J.; Demont, P.; Bernes, A.; Lacabanne, C. *J. Polym. Sci. Part B: Polym. Phys.* **1999,** *37*, 3494.

24. Vigier, G.; Tatibouet, J.; Benatmane, A.; Vassoille, R. *Colloid Polym. Sci.* **1992,** *270*, 1182.

25. Kressmann, R.; Sessler, G. M.; Gunther, P. *IEEE Trans. Dielectr. Electr. Insul.* **1996,** *3*, 607.

26. Menczel, J.; Wunderlich, B. *Abstr. Pap. Am. Chem. Soc.* **1986,** *191*, 93.

27. Kattan, M.; Dargent, E.; Grenet, J. *J. Therm. Anal. Calorim.* **2004,** *76*, 379.

28. Chen, H. P.; Cebe, P. *Macromolecules* **2009,** *42*, 288.

29. Schmieder, K.; Wolf, K. *Colloid Polym. Sci.* **1953,** *134*, 149.

30. Bernes, A.; Chatain, D.; Lacabanne, C. *Polymer* **1992,** *33*, 4682.

31. Boyd, R. H. *J. Chem. Phys.* **1959,** *30*, 1276.

32. McCrum, N. G.; Read, B. E.; Williams, G. Anelastic and Dïelectric Effects in Polymeric Solids; Wiley: London, **1967.**

33. Pathmanathan, K.; Cavaille, J. Y.; Johari, G. P. *J. Polym. Sci. Part B: Polym. Phys.* **1992,** *30*, 341.

34. Dantras, E.; Dudognon, E.; Samouillan, V.; Menegotto, J.; Bernes, A.; Demont, P.; Lacabanne, C. *J. Non-Cryst. Solids* **2002,** *307*, 671.